



Cs-Cu-Cl perovskite quantum dots for photocatalytic H₂ evolution with super-high stability



Yuanli Li^a, Chunqiang Zhuang^{a,*}, Shi Qiu^b, Junfeng Gao^b, Quan Zhou^a, Zaicheng Sun^{c,*}, Zhenhui Kang^{d,e, **}, Xiaodong Han^a

^a Institute of Microstructure and Property of Advanced Materials, Faculty of Materials and Manufacturing, Beijing University of Technology, Beijing 100124, China

^b Key Laboratory of Material Modification by Laser, Ion and Electron Beams, School of Physics and DUT-BSU Joint Institute, Dalian University of Technology, Dalian 116024 China

^c Center of Excellence for Environmental Safety and Biological Effects, Beijing Key Laboratory for Green Catalysis and Separation, Department of Chemistry, Faculty of Environment and Life, Beijing University of Technology, Beijing 100124, China

^d Institute of Functional Nano and Soft Materials (FUNSOM), Jiangsu Key Laboratory for Carbon-based Functional Materials and Devices, Soochow University, Suzhou 215123, China

^e Macao Institute of Materials Science and Engineering (MIMSE), MUST-SUDA Joint Research Center for Advanced Functional Materials, Macau University of Science and Technology, Taipa 999078, Macao

ARTICLE INFO

Keywords:

Single-component perovskite
All-in-one
Quantum dot
Water-stable
Photocatalysis

ABSTRACT

Metal halide perovskites with broad optical absorption and long carrier lifetime are considered as ideal photocatalysts. However, their poor stability in water greatly impedes their application in photocatalytic H₂ evolution because they lose their crystalline structure in water. Herein, we proclaim a new class of photocatalysts: all-inorganic Cs-Cu-Cl perovskite quantum dots (QDs). It exhibits a high photocatalytic hydrogen production rate of ~ 3.1 mmol/g/h without any cocatalyst under AM 1.5-G solar irradiation (100 mW/cm²). Especially, it remains the high activity for up to 330 h without apparent deterioration of the hydrogen production rate. Density functional theory (DFT) calculations reveal that the Cu site works as the electron and proton absorption sites as the H₂ production active center. To our best knowledge, there is no report of metal halide perovskites as water-stable photocatalysts. This work opens an innovative way for guiding the exploration of metal halide perovskites photocatalysts for stable photocatalytic H₂ evolution.

1. Introduction

Metal halide perovskites have been extensively investigated in recent years due to their unique properties [1–3], such as the wide light absorption from UV to the visible range with tunable bandgap [4,5], the high carrier lifetime [6,7] and the low exciton binding energy [8]. These advantages allow metal halide perovskites to be ideal photocatalysts for photocatalytic reactions [9–16]. Therefore, besides the extensive study of metal halide perovskites on optoelectronic devices, they have also been widely explored for photocatalytic reactions [17–28].

However, the exploration of metal halide perovskites for photocatalytic reactions has been severely impeded because metal halide perovskites are soluble or unstable in water [9,29,30]. They tend to

decompose into ions in water, thus their perovskite structures can be destroyed, leading to the loss of their photocatalytic activity [31,32]. To prevent their decompositions, different methods have been attempted. For example, Nam et al. used the hydriodic acid (HI) to stabilize their prepared MAPbI₃ perovskites [33]. They found that the existence of HI can maintain the dynamic equilibrium of dissolution and recrystallization. Guo et al. also found that all-inorganic Cs₂SnI₆ perovskites show a high photocatalytic hydrogen production [9]. The corresponding cycling tests display that Cs₂SnI₆ perovskites can be stable for 24 h in HI solution under light irradiation. Besides the addition of acid solution, iodine salts are also used for the stabilization of perovskites in aqueous solution. For example, Li et al. used PEA₂PbI₄ perovskites [34]. The hydrogen yield shows nearly

* Corresponding authors.

** Corresponding author at: Institute of Functional Nano and Soft Materials (FUNSOM), Jiangsu Key Laboratory for Carbon-based Functional Materials and Devices, Soochow University, Suzhou 215123, China.

E-mail addresses: chunqiang.zhuang@bjut.edu.cn (C. Zhuang), sunzc@bjut.edu.cn (Z. Sun), zhkang@suda.edu.cn (Z. Kang).

no degradation after 16 h under light irradiation. Most reported works are based on saturated halogen acid solutions to keep the stability of metal halide perovskites [5], which leads to the decomposition of a halogen acid, not the real water splitting. So far, there has been no report of metal halide perovskites that have good photocatalytic hydrogen production with superb stability in an aqueous solution. Therefore, the design of water-stable metal halide perovskites with considerable hydrogen production has been the primary goal to realize their potential photocatalytic applications.

Herein, we report a new class of all-in-one Cs-Cu-Cl perovskites as photocatalysts. Without any addition of cocatalyst, these single Cs-Cu-Cl perovskites have an excellent photocatalytic hydrogen production. Moreover, they can be stabilized in aqueous solution up to 330 h without apparent deterioration under light irradiation, reaching the record-high stability ever reported for all organic or inorganic perovskites in an aqueous solution. Density functional theory (DFT) calculations demonstrate that Cu positions act as the absorption sites of hydrogen protons for highly efficient hydrogen production.

2. Experimental section

2.1. Chemical reagents

The chemical reagents purchased were directly used without any purification. They are CuCl (99.99 % metals basis, Aladdin), CsCl (AR, Aladdin), HCl (37 %, Beihua), Lactic acid (AR, Adamas), Na₂SO₃ (98 %, Aladdin), and Citric acid (99.5 %, Macklin).

2.2. Preparation of Cs-Cu-Cl perovskite quantum dots

A total of 1 mmol of CuCl powder was dispersed into 15 mL of deionized water with ultrasonic treatment for 30 min. Then CsCl powder was added to the above solution under continuous stirring for 3 h. After the solution was completely transferred into a transparent one, Cs-Cu-Cl perovskite quantum dots was formed. By changing the added amount of CsCl (0.0 mmol, 0.5 mmol, 1 mmol, 1.5 mmol, 1.6 mmol, 1.7 mmol, 1.8 mmol, 1.9 mmol, 2.0 mmol, 3.0 mmol, 4.0 mmol, 5.0 mmol, 6.0 mmol, 7.0 mmol, 8.0 mmol), a series of Cs-Cu-Cl perovskites were obtained. They are marked as samples No. 1–15, respectively. The solution with Cs-Cu-Cl perovskites can be quickly frozen by liquid nitrogen and then dried by a freeze drier to obtain Cs-Cu-Cl powders for the succeeding characterization of X-ray diffraction. The solution can also be directly dispersed onto ultra-thin carbon films for the characterization of TEM and UV-vis spectra.

2.3. Material characterizations

The microstructure of freeze-drying Cs-Cu-Cl perovskites was characterized by an X-ray diffractometer (Bruker D8 Advance) with Cu K α radiation. Transmission electron microscopy (TEM, TALOS, F200) with high-angle angular dark field (HAADF) and Energy dispersion spectrum (EDS) was used to examine the high-resolution atomic structures and the elemental distributions. UV-Vis spectra of the solution with Cs-Cu-Cl perovskites were analyzed by a spectrophotometer (UV-2600, Shimadzu).

2.4. Photocatalytic activity evaluation

1 mmol of CuCl powder was dispersed into 30 mL of deionized water with ultrasonic treatment for 30 min to form a suspension. Then CsCl was added into the suspension under strong stirring for 3 h till the suspension turns into transparent solution. Afterward, 100 μ L of HCl as a stabilizer and 5 mL of lactic acid as the sacrificial agent were dropped into the solution under continuous stirring. The in-situ synthesized solution was then transferred into a reactor in a gas-closed system (Lab-solar 6 A, Beijing Perfectlight Technology Co., Ltd.) with the cooling

water to keep the temperature of the reactor at 5 °C, and directly utilized for photocatalytic tests. A 300 W Xe lamp was used as the light source. The incident light was tuned by an AM1.5-G filter to let the light intensity be one sun (100 mW/cm²). The corresponding diameter of the filter is 57 mm, which is equal to the diameter of light spot that can reach to the upper surface of reaction solution. The hydrogen production was analyzed by an online gas chromatograph with a TCD detector (GC-7900, Ar carrier gas). During the cycling process, no extra sacrifice agent was reintroduced.

The apparent quantum efficiency (AQE) is calculated as follows. The aqueous solution with Cs-Cu-Cl perovskite particles is transparent. This indicates that most of incident light is not adsorbed. Therefore, we used the powder of the incident light on the upper surface to subtract the light powder out of the lower surface as the actual powder of light adsorption by the solution. We used the standard 5-point method to determine the average light powder [35,36]. The energy of single photon is calculated by:

$$E_0 = h \frac{c}{\lambda} \quad (1)$$

where λ represents the wavelength of incident light, h is Planck constant, and c describes the velocity of light. The total number of photons consumed in the reaction solution is expressed by:

$$n_0 = \frac{w}{E_0} \quad (2)$$

By combining the Eq. (1) and Eq. (2), the AQE is obtained by:

$$AQE(\%) = \frac{2n_1}{n_0} \times 100\% = \frac{2n_1 hc}{w\lambda} \times 100\% \quad (3)$$

2.5. Density functional theory calculations

Density functional theory (DFT) calculations were performed by Vienna ab initio simulation package (VASP) [37,38]. Planewave basis set was used with an energy cutoff of 500 eV. The projector augmented wave (PAW) potential and the generalized gradient approximation (GGA) by Perdew, Burke and Ernzerhof (PBE) were used to treat the exchange-correlation functional [39–41]. The convergency for total energy was set to 10^{-7} eV, and the residual force on each atom of the structural models after geometric optimization was less than 0.01 eV/Å. The Brillouin zone was sampled using a uniform distribution of K-points with the spacing of 0.03/Å. A vacuum layer with the thickness of 15 Å was used along the Z direction to avoid the interaction between adjacent layers. The Gibbs free energy change (ΔG) was calculated by the following equation [42]:

$$\Delta G = E_H - \Delta E_{ZPE} - T\Delta S, \quad (4)$$

where E_H is the hydrogen chemisorption energy. ΔE_{ZPE} and ΔS is the change of zero-point energy and entropy between gas and adsorbed phase, respectively. The chemisorption energy was calculated according to the equation based on ground-state energy:

$$\Delta E_{*H} = E_{*H} - E_* - 1/2E_{H_2} \quad (5)$$

where E_* and E_{H_2} is the total energy of bare substrate and hydrogen gas, respectively. E_{*H} is the total energy of the adsorbed *H motif on the bare substrate. The overall process is summarized as follows:

The Volmer reaction (adsorption):



The Tafel/Heyrovsky reaction (desorption):



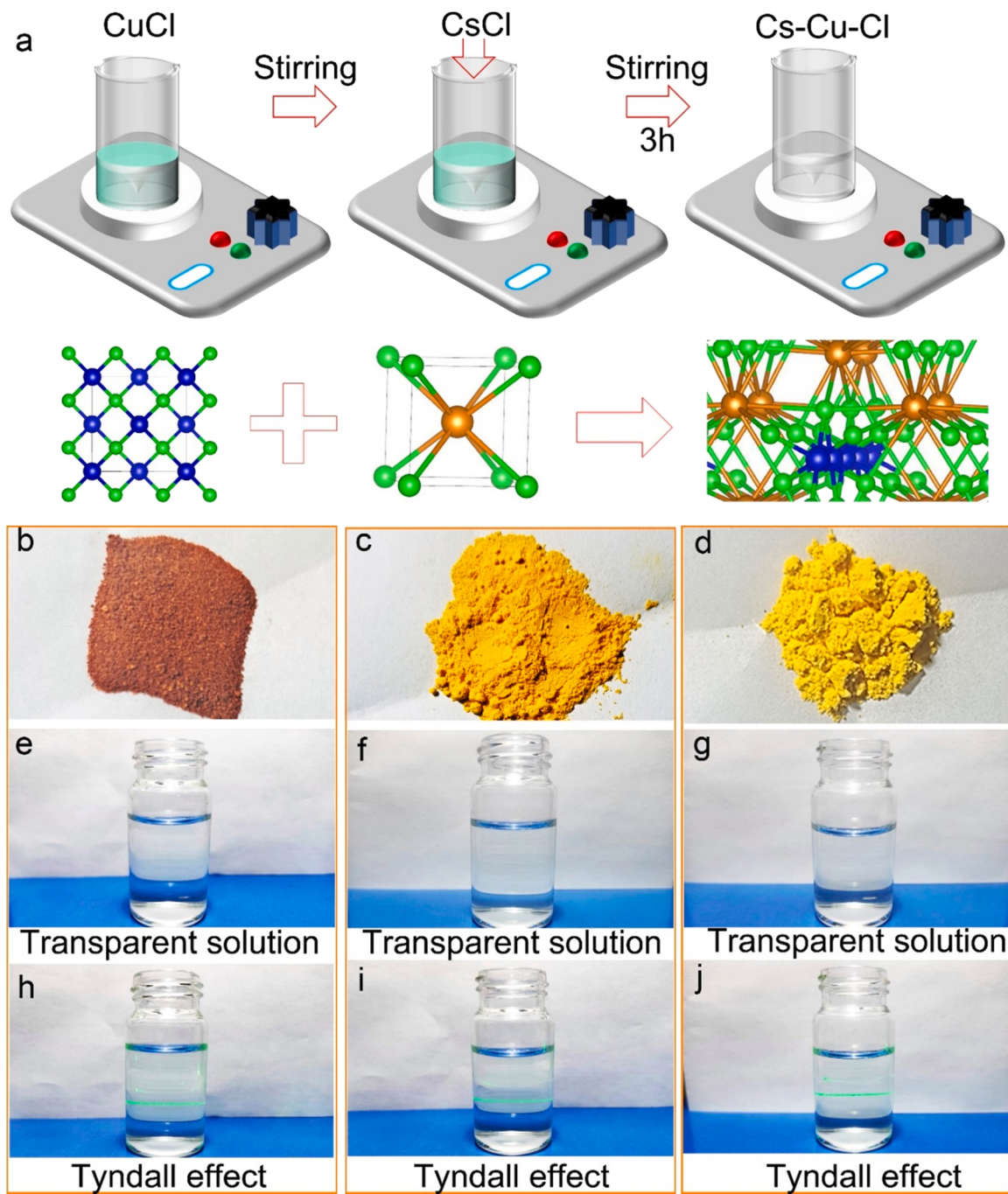


Fig. 1. (a) Schematic illustration of the in-situ construction of Cs-Cu-Cl perovskites in aqueous solution. (b-d), Digital photographs of representative freeze-drying samples obtained by adding CsCl concentrations of 5 mM, 0.1 M, and 0.4 M, respectively. (e-g), The transparent solution corresponds to (b-d), respectively. (h-j), Tyndall effect in these transparent solutions correspond to (h-j), respectively.

Where $*$ denotes the adsorption active site on substrates. Under the Normal Hydrogen Electrode, the Gibbs free energy change can be expressed as:

$$\Delta G = \Delta E_{*H} + 0.24 \text{ eV} \quad (9)$$

3. Results and discussion

3.1. In-situ synthesis of Cs-Cu-Cl perovskites

Cs-Cu-Cl perovskites were prepared by a very simple in-situ method. As shown in Fig. 1a, CuCl powders were firstly dispersed into deionized water under magnetic stirring to form a suspension. Then designed

amount of CsCl powders was added to the suspension. After continuous stirring for 3 h, a Cs-Cu-Cl perovskite solution was obtained. By changing the added CsCl amount, a series of Cs-Cu-Cl perovskites were formed in the solution. Fig. 1b-d show three representative freeze-drying Cs-Cu-Cl perovskites. The color of these Cs-Cu-Cl perovskites changes from dark brown to light yellow as the added CsCl powders increase. However, clear transparent solutions are observed for all samples when they were dissolved into the deionized water as shown in Fig. 1e-g. With the irradiation of a laser pointer, the green beam path is observed as shown in Fig. 1h-j, indicating that all solutions have the typical Tyndall effect [43]. By comparison, there is no Tyndall effect in pure deionized water or CsCl solution (Figs. S1-2). That indicates that there exist small

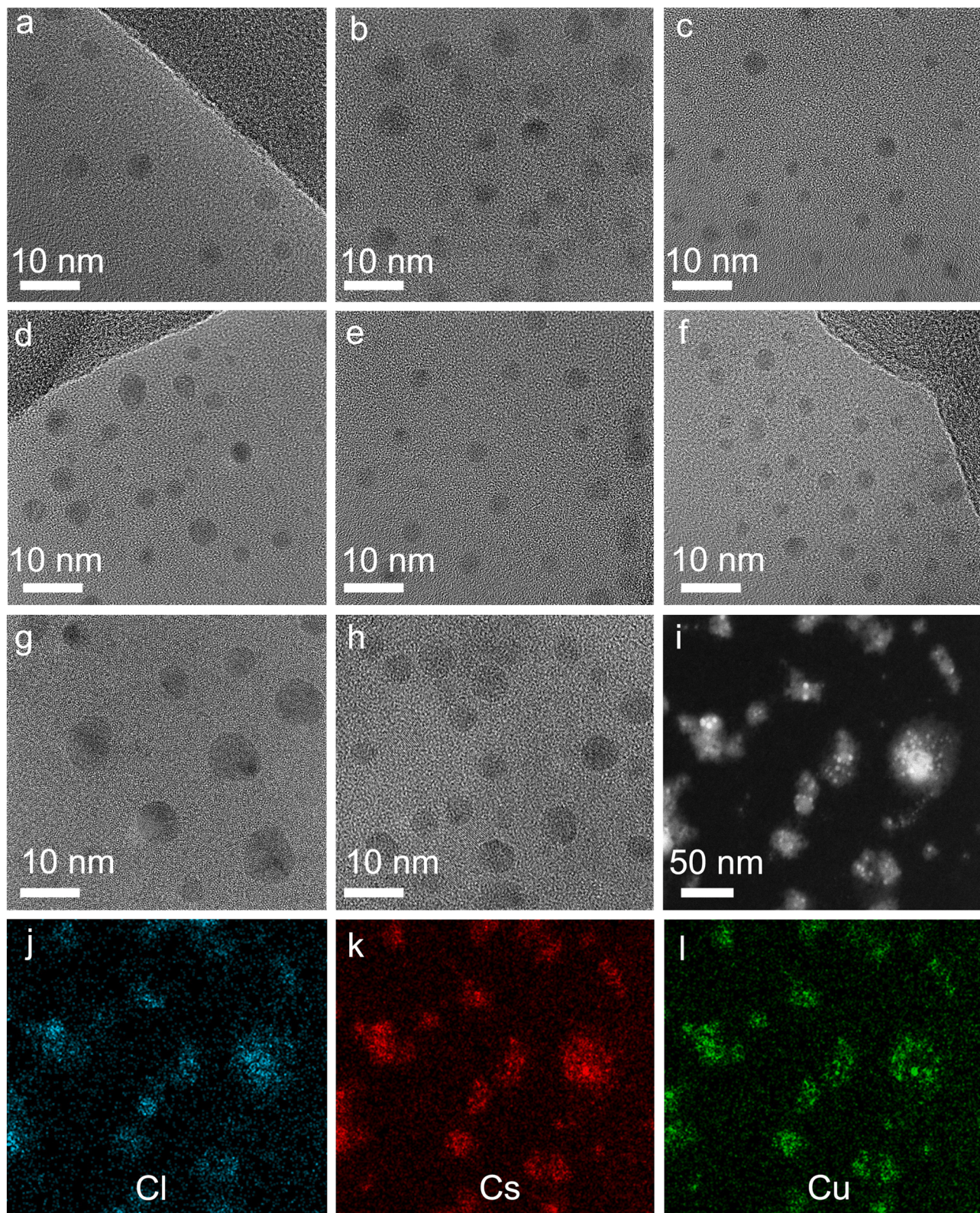


Fig. 2. (a-h), Representative TEM images of samples No. 3, No. 5, No. 7, No. 9, No. 10, No. 11, No. 13 and No. 15 by directly dispersing their transparent aqueous solutions onto ultra-thin carbon films supported by copper grids. Quantum dots can be observed. (i), High-angle annular dark field (HAADF) scanning transmission electron microscopy (STEM) image of sample No. 9. (j-l), The corresponding energy dispersion spectroscopy (EDS) elemental maps of Cs, Cl, and Cu, respectively. EDS maps demonstrate that these small particles are Cs-Cu-Cl perovskite quantum dots.

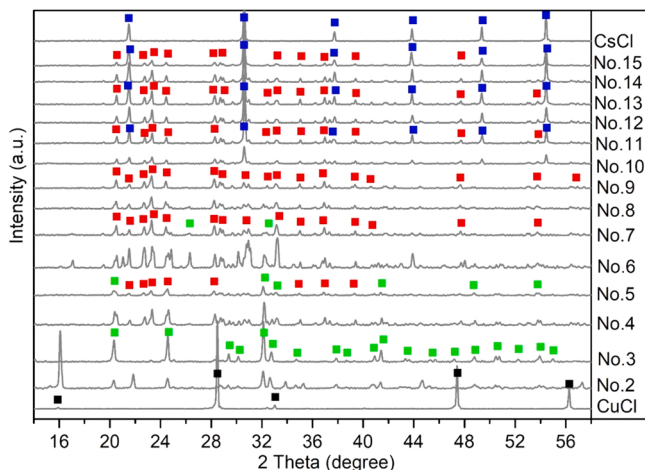


Fig. 3. X-ray diffraction (XRD) of Cs-Cu-Cl perovskite quantum dots. The XRD patterns of CuCl and CsCl are also shown for comparison. The XRD pattern of sample No. 3 and No. 9 corresponds to the pure phase of CsCuCl_3 and Cs_2CuCl_4 , respectively.

particles in the solution. As mentioned above, the CuCl is slightly soluble in deionized water with a solubility product of 1.7×10^{-7} , in which CuCl precipitations can also be observed (Fig. S3). When CsCl aqueous solution is added to the CuCl dispersion, the CuCl solid gradually disappears. Therefore, these newly formed transparent solutions indicate that CsCl has reacted with CuCl to form Cs-Cu-Cl perovskites in the

solution. In addition, our work is different from previous reported one [34], in which iodine salts were added and used as stabilizer. In our case, the added CsCl was used as the precursor to react with CuCl to form Cs-Cu-Cl perovskite materials, and CsCl was not deliberately used as a stabilizer.

3.2. Microstructural characterizations

To examine the existing form of Cs-Cu-Cl perovskites in these newly formed transparent solutions, transmission electron microscopy (TEM) was employed. Newly formed transparent solutions with in-situ synthesized Cs-Cu-Cl perovskites were directly dropped onto ultra-thin carbon films supported on copper grids and then sucked away by filter papers, leaving possible residues on ultra-thin carbon films. Fig. 2a-h show TEM images of several representative samples. Small particles with a grain size of less than 10 nm can be observed for all these transparent solutions. Fig. 2i-l further verify that these small particles are Cs-Cu-Cl perovskites, demonstrating that these transparent solutions with Tyndall effects contain Cs-Cu-Cl perovskite quantum dots.

To further identify their microstructures, X-ray diffraction (XRD) was employed to study possible crystal phases in these Cs-Cu-Cl perovskites based on freeze-drying samples. Fig. 3 shows some representative XRD patterns of Cs-Cu-Cl perovskites. The XRD patterns of pure CuCl and CsCl are also shown for comparison. It can be seen from the XRD patterns that the crystal phase changes from CuCl (PDF#82-2114) to CsCuCl_3 (PDF#73-1467) (No. 3) with the addition of CsCl by 5 mM. Further increase of the CsCl concentration up to 20 mM, a new crystal phase of Cs_2CuCl_4 (PDF#24-1335) is formed. The two crystal phases

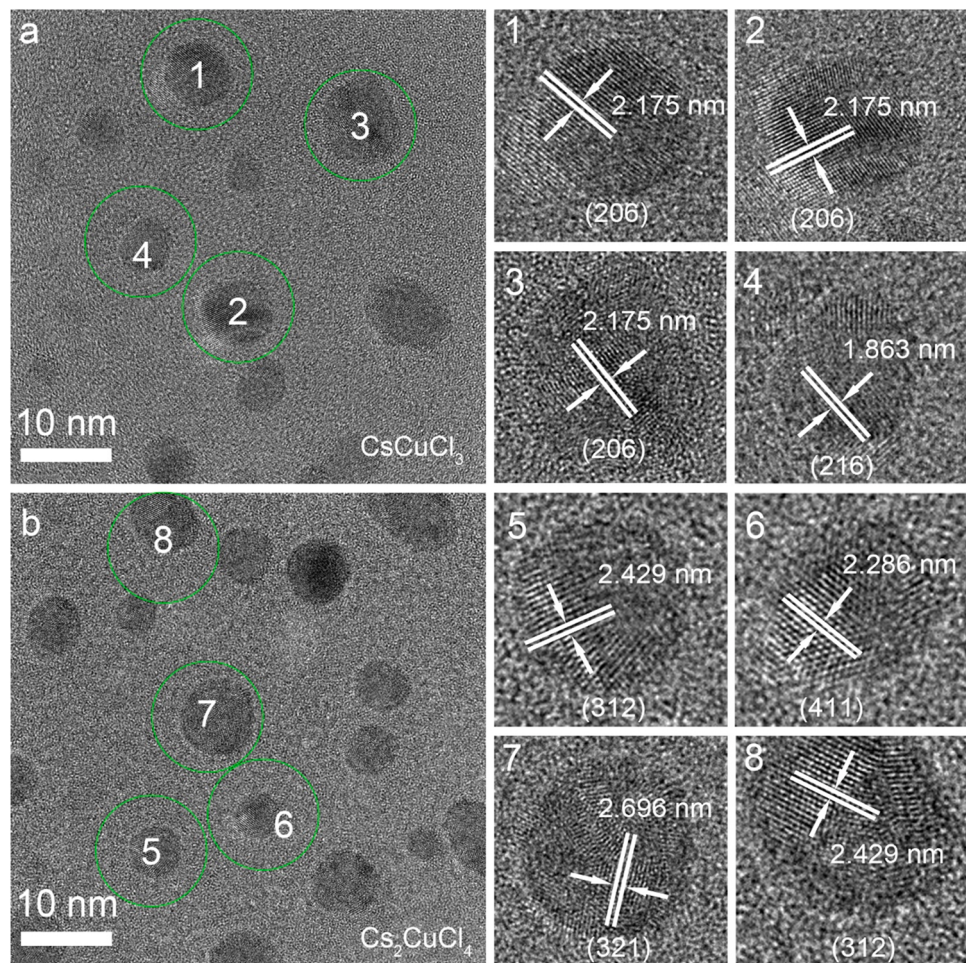


Fig. 4. High-resolution TEM images of freeze-dried samples No. 3 (a) and No. 9 (b) and their high magnification particles with clear lattice fringes.

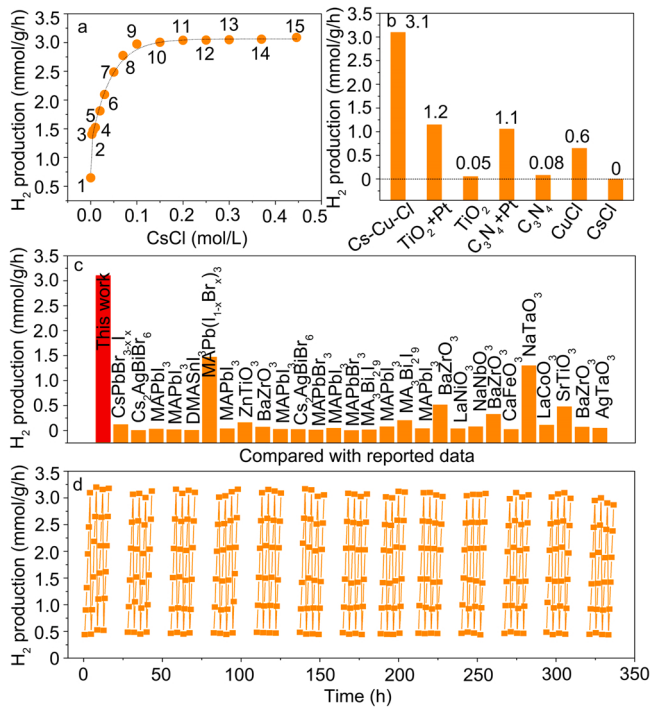


Fig. 5. (a) Photocatalytic hydrogen production of Cs-Cu-Cl perovskites as a function of the added CsCl concentration. The corresponding samples are labeled as No. 1–15, respectively. (b) Photocatalytic hydrogen production for different single-component photocatalysts. (c) Quantum efficiency of sample No. 9 with the pure crystal phase of Cs₂CuCl₄. (d) Comparison of photocatalytic hydrogen production of our Cs-Cu-Cl perovskite with reported data. Almost all perovskites for photocatalytic hydrogen evolution are included. (e) Record-high cycling stability of our perovskite in aqueous solution.

coexist in the sample (No. 5). As the added CsCl concentration increases up to 50 mM, the CsCuCl₃ phase is gradually transferred into the Cs₂CuCl₄ phase (No. 7). At the CsCl concentration of 0.1 M, the CsCuCl₃ phase has been almost completely transferred into Cs₂CuCl₄ phase (No. 9). The subsequent CsCl addition does not change the Cs₂CuCl₄ crystalline phase, indicating that CsCl has been excess. All XRD patterns of Cs-Cu-Cl perovskites after sample No. 9 show the characteristic peaks of CsCl (PDF#05-0607), as can be observed from the XRD patterns of sample No. 11, No. 13, and No. 15 in Fig. 3. Based on these XRD data, we can conclude that there exist phase transformations from CuCl to CsCuCl₃, and Cs₂CuCl₄ with the continuous addition of CsCl.

To directly observe these existing crystal phases, Fig. 4 shows high-resolution TEM images of two representative samples with pure crystal phases (No. 3 and No. 9). Perovskite quantum dots can also be observed after redispersing freeze-drying samples into aqueous solution. To see their lattice fringes, some representative particles as indicated by green circles are magnified. The particles marked with No. 1–4 show a lattice spacing of 2.175 nm, 2.175 nm, 2.175 nm, and 1.863 nm, respectively. They correspond to the (206), (206), (206), and (216) planes of CsCuCl₃ quantum dots. Similarly, the particles marked with No. 5–8 show the lattice spacing of 2.429 nm, 2.286 nm, 2.696 nm, and 2.429 nm, respectively. They correspond to the (312), (411), (321) and (312) planes of Cs₂CuCl₄ quantum dots. These HR-TEM images demonstrate that Cs-Cu-Cl perovskites indeed exist in the manner of dispersed small particles in reactive aqueous solution, and they are in accord with XRD results.

3.3. Photocatalytic H₂ production with superstability

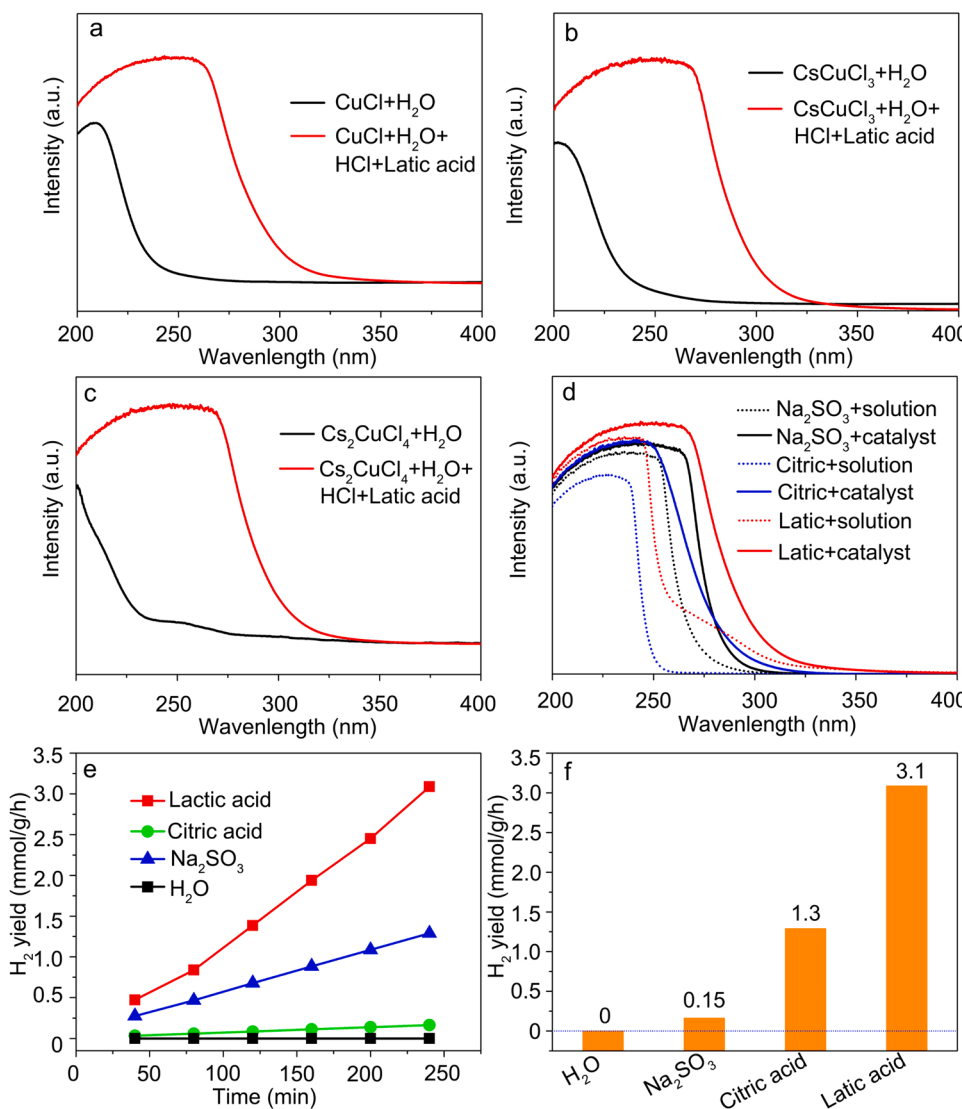
To evaluate photocatalytic properties, in-situ synthesized Cs-Cu-Cl perovskites were directly utilized. They are respectively marked by

the number from No. 1 to No. 15 in Fig. 5a. As shown in Fig. 5a, the photocatalytic hydrogen production increases as the CsCl concentration increases. As the CsCl concentration increases up to 0.1 M (No. 9), the hydrogen yield reaches up to a platform, and it is almost unchanged with further increase of the CsCl concentration. The maximum hydrogen yield is ~ 3.1 mmol/g/h (No. 15).

Fig. 5b shows the comparison of hydrogen yield between our optimized Cs-Cu-Cl perovskite and two typical photocatalysts: TiO₂ and graphitic C₃N₄. The hydrogen yield for pure TiO₂ and graphitic C₃N₄ is ~ 0.05 mmol/g/h and ~ 0.08 mmol/g/h, respectively, comparable to the reported data [21,44–48]. After Pt loading, it is ~ 1.2 mmol/g/h and ~ 1.1 mmol/g/h, respectively, which is still far less than that of our Cs-Cu-Cl sample. The optimized Cs-Cu-Cl sample contains pure Cs-Cu-Cl perovskites and excess CsCl. However, pure CsCl shows no hydrogen yield (Fig. S4). Therefore, the hydrogen production only originates from the pure single-component Cs-Cu-Cl perovskite. These results indicate that single-component metal halide perovskites without any cocatalyst can also exhibit excellent photocatalytic properties for hydrogen evolution in an aqueous solution. We also performed photocatalytic hydrogen evolution using the sample No. 9 (Cs₂CuCl₄) with Pt photo-deposition. As shown in Fig. S5, the hydrogen yield is nearly the same, indicating that the introduction of Pt source does not contribute to significantly improving the H₂ yield. In addition, the oxidation products were also examined by nuclear magnetic resonance (NMR) as shown in Figs. S6–S7.

In addition, we also notice that the photocatalytic hydrogen production of sample No. 9 with the dominated Cs₂CuCl₄ phase is obviously higher than that of the sample No. 3 with the dominated CsCuCl₃ phase. We attempt to explore the possible reason from the perspective of their structures. Fig. S8 shows the XPS spectra of Cs₂CuCl₄ and CsCuCl₃ phase. Cu, Cs, and Cl signals can be observed from the full spectra as shown in Fig. S8a and S8c, verifying that they are Cs-Cu-Cl perovskite materials. However, the high-resolution XPS of Cu_{2p} shows greatly difference. For CsCuCl₃, the dominated valence state for Cu ions is Cu²⁺, only few Cu⁺ ions can be observed from the high-resolution XPS (Fig. S8b). However, For Cs₂CuCl₄, the Cu⁺ valence state for Cu ions is noticeable. They coexist with Cu²⁺ ions in Cs₂CuCl₄. Because Cu⁺ and Cu²⁺ contained species (such as Cu₂O, CuO) are good cocatalysts for photocatalytic H₂ evolution, the synergistic effect of Cu⁺ and Cu²⁺ may probably be responsible for the higher photocatalytic H₂ production of Cs₂CuCl₄ comparing with that of CsCuCl₃. Meanwhile, the steady-state PL spectra in Fig. S9 show that the charge separation in Cs₂CuCl₄ is more efficient. Moreover, the transient PL characterizations in Fig. S10 indicate that the carrier lifetime in Cs₂CuCl₄ is also longer, which is beneficial for effective photo-generated electrons participating in photocatalytic hydrogen evolution.

The corresponding quantum efficiency (QE) is shown in Fig. 5c based on sample No. 9, which is a pure Cs₂CuCl₄ crystal phase. The QE is as high as ~ 90%, clearly demonstrating the high efficiency of photon conversion. To further demonstrate the exceptional photocatalytic properties of Cs-Cu-Cl perovskites, nearly all perovskites reported for photocatalytic hydrogen are collected in Fig. 5d for comparison. The detailed information is shown in Table S1. Our single-component Cs-Cu-Cl sample has the highest hydrogen yield among all reported data. Moreover, our single-component Cs-Cu-Cl sample shows a record-high cycling stability in an aqueous solution. As shown in Fig. 5e, the hydrogen yield still keeps nearly the same after 330 h, strongly demonstrating that single-component all-inorganic Cs-Cu-Cl perovskites have superb cycling stabilities for the application of photocatalytic hydrogen evolution. In addition, we also checked the Cs-Cu-Cl perovskite quantum dots after cycling experiments. As shown in Fig. S11, Cs-Cu-Cl perovskite quantum dots can also be evidently identified although they do not have clear contour profiles due to the covered organic molecules.



3.4. Light absorption

To understand the potential photocatalytic mechanism, Light absorption is first investigated since it is one of the critical steps for photocatalytic reactions. Because UV-Vis spectrometry can be directly used to detect light absorption, here we study the ability of light absorption based on several representative samples in reaction solutions. Fig. S12 shows the UV-Vis spectra of pure water and CsCl in pure water. Nearly no light absorption is observed for the wavelength between 220 nm and 400 nm. For pure CuCl in pure water, the light absorption starts from \sim 250 nm as shown in Fig. 6a. However, the light absorption shifts towards a higher wavelength of \sim 350 nm with the addition of lactic acid. Another representative Cs-Cu-Cl perovskite quantum dots, CsCuCl₃ (Fig. 6b) and Cs₂CuCl₄ (Fig. 6c), show a similar trend as that of the pure CuCl. According to our photocatalytic experiments, CuCl, CsCuCl₃ or Cs₂CuCl₄ in pure water has no photocatalytic hydrogen yield. Only after the addition of lactic acid, did they show an obvious hydrogen yield. This indicates that lactic acids not only play the role of sacrificial agent but also link with perovskite quantum dots to make their light absorption shift towards high wavelengths. We also performed repeated photocatalytic experiments to demonstrate the importance of lactic acid. If the photocatalytic experiment was performed in pure water, there is no H₂ yield that can be detected. This indicates that there is no effective photoelectron that can be extracted for H₂ evolution. By further adding

10 μ L of lactic acid, H₂ yield can be clearly detected as shown in Fig. S13. Then the reaction solution was directly frozen drying by a freeze drier, and the corresponding sample was redispersed into pure water for photocatalytic H₂ evolution. Again, there is no H₂ yield. In contrast, H₂ yield can be obtained by further addition of lactic acid. These repeated experiments verify the importance of lactic acid.

To confirm the linkage between organic molecules and perovskite quantum dots, we used citric acid as another organic and Na₂SO₃ as the pure inorganics. As can be seen from Fig. 6d, the initial light absorption for Na₂SO₃ in water and Na₂SO₃ with Cs₂CuCl₄ in water is nearly the same. This indicates that the Na₂SO₃ aqueous solution does not contribute to the light absorption of perovskite quantum dots. It is only used as the sacrificial agent, which is obviously different from citric acid and lactic acid. Their photocatalytic hydrogen yields as a function of reaction time are shown in Fig. 6e, and the corresponding hydrogen yield for 4 h is summarized in Fig. 6f. For Cs₂CuCl₄ in pure water, there is no hydrogen yield. For pure Na₂SO₃ inorganics without linkage with perovskite quantum dots, the hydrogen yield is \sim 0.15 mmol/g/h. However, the hydrogen yield reaches up to \sim 3.1 mmol/g/h with the addition of lactic acid, \sim 20 times higher than that of perovskite quantum dots with Na₂SO₃ inorganics. This strongly demonstrates that the linkage between Lactic acid and perovskite quantum dots strengthens the light absorption of perovskite quantum dots. Meanwhile, Lactic acid in the reaction solution also acts as the sacrificial

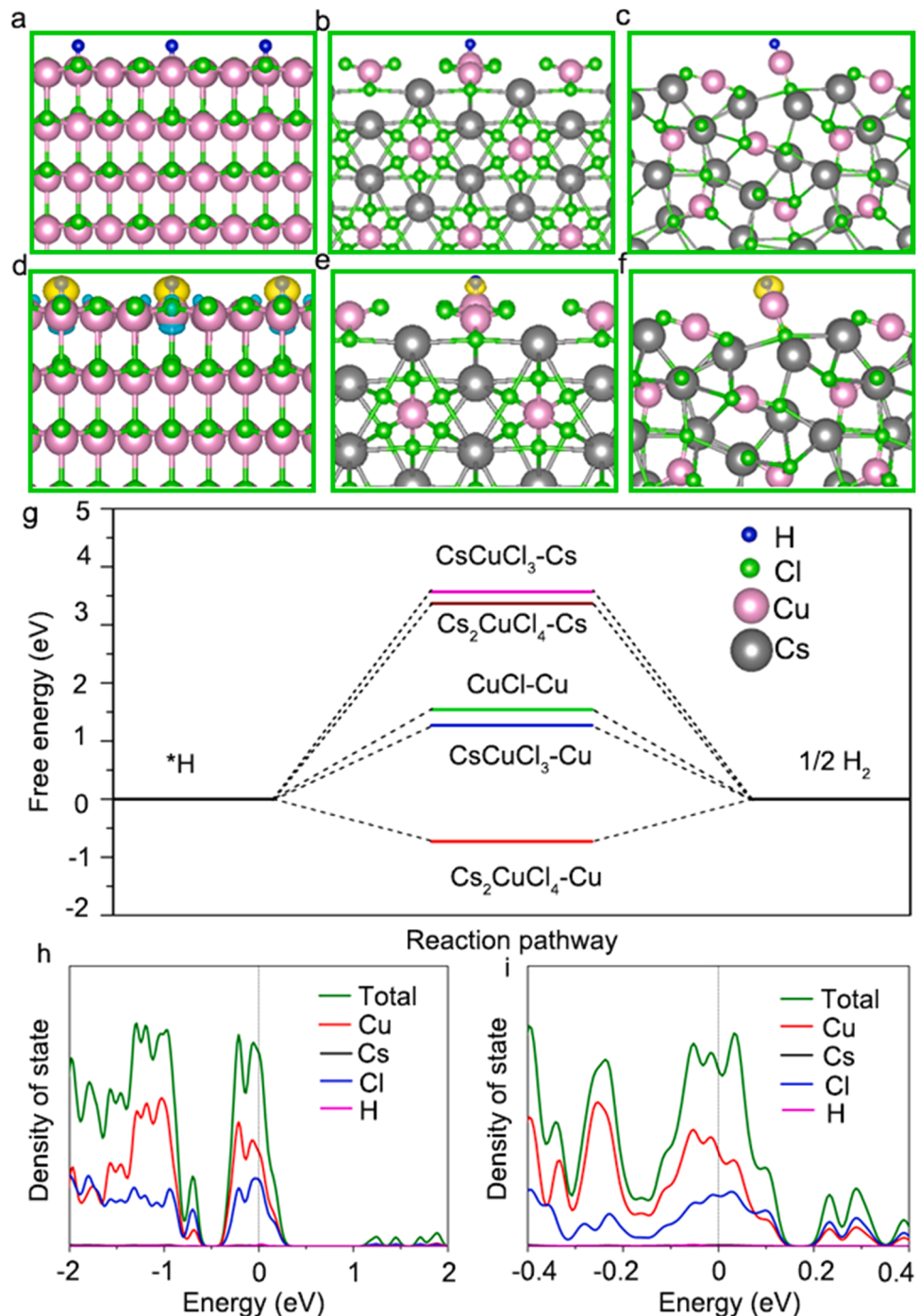


Fig. 7. Photocatalytic mechanism study by DFT calculations. Hydrogen adsorption on exposed Cu sites of CuCl (a), CsCuCl₃ (b) and Cs₂CuCl₄ (c). The differential charge density of CuCl (d), CsCuCl₃ (e) and Cs₂CuCl₄ (f) with exposed Cu surfaces. g, Free energy calculations of CuCl, CsCuCl₃ and Cs₂CuCl₄ with hydrogen adsorption on Cu or Ce exposed sites. h, Partial density of states for CsCuCl₃. i, Partial density of states for Cs₂CuCl₄.

agent to consume photo-generated holes, thus realizing highly efficient photocatalytic hydrogen evolution.

3.5. Identification of active centers

To identify potential active centers, density functional theory (DFT) calculations were performed. There only exist three different crystal phases that can be used for photocatalytic hydrogen evolution, namely, CuCl, CsCuCl₃ and Cs₂CuCl₄. Therefore, their structural models were constructed. Fig. 7a-c show optimized structural models for the hydrogen adsorption on Cu sites of CuCl, CsCuCl₃ and Cs₂CuCl₄,

respectively. The hydrogen adsorption on Cs sites was also considered in Figs. S14-15. The corresponding differential charge densities are shown in Fig. 7d-f, respectively. All these differential charge densities show a strong coupling between adsorbed hydrogen and underlying Cu sites, indicating that there exists strong interaction between hydrogen and Cu sites. This is beneficial to rapid charge transfer and highly efficient hydrogen evolution. The free energy in Fig. 7g shows that the adsorption of hydrogen on Cs sites has relatively high free energy, indicating that it is difficult to separate hydrogen from water on Cs sites. In contrast, the low value of the free energy for the hydrogen adsorption on Cu sites contributes to hydrogen evolution. Among them, the hydrogen

adsorption on Cu sites in Cs_2CuCl_4 perovskite quantum dots has negative free energy, indicating that H adsorption on the Cs_2CuCl_4 is a spontaneous process. This is consistent with the data shown in Fig. 5a. That is, with the addition of CsCl , Cs_2CuCl_4 perovskite quantum dots become dominant, corresponding to higher photocatalytic hydrogen yield. In addition, the partial density of states (PDOS) for CsCuCl_3 and Cs_2CuCl_4 is shown in Fig. 7h-i, respectively. Both PDOS show that Cu and Cl dominate the density of states near the Fermi level, further verifying Cu sites as potential charge transfer channels. Therefore, single-component Cs-Cu-Cl perovskite quantum dots with Cu sites as active centers can greatly promote photocatalytic hydrogen evolution.

3.6. Potential photocatalytic mechanism

Based on above-mentioned experimental and theoretical data, we proposed a possible mechanism for photocatalytic H_2 evolution. Under simulated light irradiation, Cs-Cu-Cl perovskites are excited and photogenerated electrons jump from the valence band to its conductive band to realize the charge separation. Then photogenerated electrons transfer to the surface of Cs-Cu-Cl perovskites, and proceed towards the exposed Cu sites for the photocatalytic hydrogen evolution. Photogenerated holes are consumed on the surface of Cs-Cu-Cl perovskites by sacrifice agent and possibly oxidized into iso-butyl acetate, acetic acid, and acetonitrile (Figs. S13-S14). Due to the small size of Cs-Cu-Cl perovskite quantum dots, photogenerated electrons can easily move to their surfaces for highly efficient photocatalytic hydrogen evolution.

4. Conclusion

Using a very simple in-situ method, we have successfully synthesized all-inorganic Cs-Cu-Cl perovskite quantum dots. These perovskite quantum dots can realize the record-high stability of photocatalytic hydrogen evolution in aqueous solution. This work breaks the routine understanding of all-inorganic perovskites that are not suitable as photocatalysts for hydrogen evolution due to their dissolution into ion states in an aqueous solution. This work also represents a significant step toward the broad exploration of new kinds of all-inorganic perovskites as photocatalysts.

CRediT authorship contribution statement

Yuanli Li: Investigation, Data curation. **Chunqiang Zhuang:** Conceptualization, Supervision, Writing- Reviewing and Editing. **Shi Qiu:** Software. **Junfeng Gao:** Software. **Quan Zhou:** Investigation. **Zaicheng Sun:** Conceptualization, Supervision. **Zhenhui Kang:** Conceptualization, Supervision. **Xiaodong Han:** Conceptualization, Supervision.

Declaration of Competing Interest

The authors declare that they have no known competing financial interests or personal relationships that could have appeared to influence the work reported in this paper.

Data availability

Data will be made available on request.

Acknowledgments

This work was supported by the National Natural Science Foundation of China (No. 12274011, 11874001), the Beijing Outstanding Young Scientists Projects (BJWZYJH01201910005018), the Basic Science Center Program for Multiphase Evolution in Hypergravity of the National Natural Science Foundation of China (No. 51988101).

Appendix A. Supporting information

Supplementary data associated with this article can be found in the online version at doi:10.1016/j.apcatb.2023.122881.

References

- [1] W. Zhang, G.E. Eperon, H.J. Snaith, Metal halide perovskites for energy applications, *Nat. Energy* 1 (2016), 16048.
- [2] X.-K. Liu, W. Xu, S. Bai, Y. Jin, J. Wang, R.H. Friend, F. Gao, Metal halide perovskites for light-emitting diodes, *Nat. Mater.* 20 (2021) 10–21.
- [3] P. Yang, G. Liu, B. Liu, X. Liu, Y. Lou, J. Chen, Y. Zhao, All-inorganic Cs_2CuX_4 ($\text{X}=\text{Cl}, \text{Br}$, and Br/I) perovskite quantum dots with blue-green luminescence, *Chem. Commun.* 54 (2018) 11638–11641.
- [4] Y. Dong, Y. Zou, J. Song, X. Song, H. Zeng, Recent progress of metal halide perovskite photodetectors, *J. Mater. Chem. C* 5 (2017) 11369–11394.
- [5] H. Huang, B. Pradhan, J. Hofkens, M.B.J. Roeffaers, J.A. Steele, Solar-driven metal halide perovskite photocatalysis: design, stability, and performance, *ACS Energy Lett.* 5 (2020) 1107–1123.
- [6] Y. Xu, M. Cao, S. Huang, Recent advances and perspective on the synthesis and photocatalytic application of metal halide perovskite nanocrystals, *Nano Res.* 14 (2021) 3773–3794.
- [7] J. Chen, C. Dong, H. Idriss, O.F. Mohammed, O.M. Bakr, Metal halide perovskites for solar-to-chemical fuel conversion, *Adv. Energy Mater.* 10 (2020), 1902433.
- [8] X. Qi, Y. Zhang, Q. Ou, S.T. Ha, C.W. Qiu, H. Zhang, Y.B. Cheng, Q. Xiong, Q. Bao, Photonics and optoelectronics of 2D metal-halide perovskites, *Small* 14 (2018), 1800682.
- [9] P. Zhou, H. Chen, Y. Chao, Q. Zhang, W. Zhang, F. Lv, L. Gu, Q. Zhao, N. Wang, J. Wang, S. Guo, Single-atom $\text{Pt}-\text{I}_3$ sites on all-inorganic Cs_2SnI_6 perovskite for efficient photocatalytic hydrogen production, *Nat. Commun.* 12 (2021) 4412.
- [10] S. Tasleem, M. Tahir, Recent progress in structural development and band engineering of perovskites materials for photocatalytic solar hydrogen production: a review, *Int. J. Hydrog. Energy* 45 (2020) 19078–19111.
- [11] Z. Zhao, J. Wu, Y.-Z. Zheng, N. Li, X. Li, Z. Ye, S. Lu, X. Tao, C. Chen, Stable hybrid perovskite $\text{MAPb}(\text{I}_{1-x}\text{Br}_x)_3$ for photocatalytic hydrogen evolution, *Appl. Catal. B: Environ.* 253 (2019) 41–48.
- [12] J. Zhong, Y. Li, H. Zhang, Z. Zhang, K. Qi, H. Zhang, C. Gao, Y. Li, L. Wang, Z. Sun, C. Zhuang, X. Han, Highly efficient charge transfer from small-sized cadmium sulfide nanosheets to large-scale nitrogen-doped carbon for visible-light dominated hydrogen evolution, *J. Colloid Interf. Sci.* 630 (2023) 260–268.
- [13] S. Yu, X. Cheng, Y. Wang, B. Xiao, Y. Xing, J. Ren, Y. Lu, H. Li, C. Zhuang, G. Chen, High activity and selectivity of single palladium atom for oxygen hydrogenation to H_2O_2 , *Nat. Commun.* 13 (2022) 4737.
- [14] K. Qi, C. Zhuang, M. Zhang, P. Gholami, A. Khataee, Sonochemical synthesis of photocatalysts and their applications, *J. Mater. Sci. Technol.* 123 (2022) 243–256.
- [15] B. Jing, Z. Ao, W. Zhao, Y. Xu, Z. Chen, T. An, Evaluation procedure of photocatalysts for VOCs degradation from the view of density functional theory calculations: $\text{g}-\text{C}_3\text{N}_4$ dots/graphene as an example, *J. Mater. Chem. A* 8 (2020) 20363–20372.
- [16] C. Zhuang, W. Li, T. Zhang, J. Li, Y. Zhang, G. Chen, H. Li, Z. Kang, J. Zou, X. Han, Monodispersed aluminum in carbon nitride creates highly efficient nitrogen active sites for ultra-high hydrogen peroxide photoproduction, *Nano Energy* 108 (2023), 108225.
- [17] Y. Wu, P. Wang, Z. Guan, J. Liu, Z. Wang, Z. Zheng, S. Jin, Y. Dai, M.-H. Whangbo, B. Huang, Enhancing the photocatalytic hydrogen evolution activity of mixed-halide perovskite $\text{CH}_3\text{NH}_3\text{PbBr}_{3-x}\text{I}_x$ achieved by bandgap funneling of charge carriers, *ACS Catal.* 8 (2018) 10349–10357.
- [18] M. Wang, Y. Zuo, J. Wang, Y. Wang, X. Shen, B. Qiu, L. Cai, F. Zhou, S.P. Lau, Y. Chai, Remarkably enhanced hydrogen generation of organolead halide perovskites via piezocatalysis and photocatalysis, *Adv. Energy Mater.* 9 (2019), 1901801.
- [19] C. Gao, Y. Li, Z. Zhang, W. Li, J. Zhong, H. Zhang, Y. Zhang, L. Deng, Z. Sun, G. Chen, H. Zhang, L. Wang, C. Zhuang, X. Han, Improving photocatalytic hydrogen production via ultrafine-grained precipitates formed nearby surface defects of NiFe-LDH nanosheets, *Chem. Eng. J.* 446 (2022), 137301.
- [20] H. Zhang, Y. Li, W. Li, C. Zhuang, C. Gao, W. Jiang, W. Sun, K. Qi, Z. Sun, X. Han, Designing large-sized cocatalysts for fast charge separation towards highly efficient visible-light-driven hydrogen evolution, *Int. J. Hydrog. Energy* 46 (2021) 28545–28553.
- [21] W. Li, C. Zhuang, Y. Li, C. Gao, W. Jiang, Z. Sun, K. Qi, Anchoring ultra-small TiO_2 quantum dots onto ultra-thin and large-sized Mxene nanosheets for highly efficient photocatalytic water splitting, *Ceram. Int.* 47 (2021) 21769–21776.
- [22] Y. Cheng, Y. Liu, C. Chu, Y. Liu, Y. Li, R. Wu, J. Wu, C. Zhuang, Z. Kang, H. Li, Carbon armour with embedded carbon dots for building better supercapacitor electrodes, *Nano Res.* (2022).
- [23] Y. Guo, G. Liu, Z. Li, Y. Lou, J. Chen, Y. Zhao, Stable lead-free $(\text{CH}_3\text{NH}_3)_3\text{BiI}_6$ perovskite for photocatalytic hydrogen generation, *ACS Sustain. Chem. Eng.* 7 (2019) 15080–15085.
- [24] D. Yue, T. Zhang, T. Wang, X. Yan, C. Guo, X. Qian, Y. Zhao, Potassium stabilization of methylammonium lead bromide perovskite for robust photocatalytic H_2 generation, *EcoMat* 2 (2020), e12015.
- [25] T. Wang, D. Yue, X. Li, Y. Zhao, Lead-free double perovskite $\text{Cs}_2\text{AgBiBr}_6/\text{RGO}$ composite for efficient visible light photocatalytic H_2 evolution, *Appl. Catal. B: Environ.* 268 (2020), 118399.

[26] Z. Fan, X. Zhang, Y. Li, X. Guo, Z. Jin, Construct 3D NiCo-LDH/Cu₂O p-n heterojunction via electrostatic self-assembly for enhanced photocatalytic hydrogen evolution, *J. Ind. Eng. Chem.* 110 (2022) 491–502.

[27] X. Wang, Y. Li, X. Guo, Z. Jin, In situ synthesis of Ag/Ag₂O on CeO₂ for boosting electron transfer in photocatalytic hydrogen production, *J. Phys. Chem. C* 126 (2022) 13015–13024.

[28] Z. Jin, X. Li, T. Li, Y. Li, Graphdiyne (C_nH_{2n-2})-based GDY/CuI/MIL-53(Al) S-scheme heterojunction for efficient hydrogen evolution, *Langmuir* 38 (2022) 15632–15641.

[29] Y. Ji, M. She, X. Bai, E. Liu, W. Xue, Z. Zhang, K. Wan, P. Liu, S. Zhang, J. Li, In-depth understanding of the effect of halogen-induced stable 2D bismuth-based perovskites for photocatalytic hydrogen evolution activity, *Adv. Funct. Mater.* 32 (2022), 2201721.

[30] H. Zhao, K. Chordiya, P. Leukkunen, A. Popov, M. Upadhyay Kahaly, K. Kordas, S. Ojala, Dimethylammonium iodide stabilized bismuth halide perovskite photocatalyst for hydrogen evolution, *Nano Res.* 14 (2021) 1116–1125.

[31] H. Wang, X. Wang, R. Chen, H. Zhang, X. Wang, J. Wang, J. Zhang, L. Mu, K. Wu, F. Fan, X. Zong, C. Li, Promoting photocatalytic H₂ evolution on organic–inorganic hybrid perovskite nanocrystals by simultaneous dual-charge transportation modulation, *ACS Energy Lett.* 4 (2019) 40–47.

[32] Z. Zhang, Y. Liang, H. Huang, X. Liu, Q. Li, L. Chen, D. Xu, Stable and highly efficient photocatalysis with lead-free double-perovskite of Cs₂AgBiBr₆, *Angew. Chem. Int. Ed.* 58 (2019) 7263–7267.

[33] S. Park, W.J. Chang, C.W. Lee, S. Park, H.Y. Ahn, K.T. Nam, Photocatalytic hydrogen generation from hydriodic acid using methylammonium lead iodide in dynamic equilibrium with aqueous solution, *Nat. Energy* 2 (2016), 16185.

[34] H. Wang, H. Zhang, J. Wang, Y. Gao, F. Fan, K. Wu, X. Zong, C. Li, Mechanistic understanding of efficient photocatalytic H₂ evolution on two-dimensional layered lead iodide hybrid perovskites, *Angew. Chem. Int. Ed.* 60 (2021) 7376–7381.

[35] Z. Zhang, Y. Li, H. Zhang, J. Zhong, W. Li, C. Gao, H. Zhang, C. Zhuang, Ultrathin CdS nanosheets grown on N-doped carbon nanotubes with encapsulated cobalts for highly improved visible-light-driven hydrogen production, *ACS Appl. Energy Mater.* 5 (2022) 15680–15688.

[36] Z. Zhang, Y. Li, J. Zhong, H. Zhang, C. Gao, C. Zhuang, N-doped carbon nanofibers coupled with TiO₂ quantum dots for photocatalytic hydrogen production, *ACS Appl. Nano Mater.* 6 (2023) 453–460.

[37] W. Kohn, L.J. Sham, Self-consistent equations including exchange and correlation effects, *Phys. Rev.* 140 (1965) A1133–A1138.

[38] G. Kresse, J. Hafner, Ab initio molecular dynamics for liquid metals, *Phys. Rev. B* 47 (1993) 558–561.

[39] P.E. Blöchl, Projector augmented-wave method, *Phys. Rev. B* 50 (1994) 17953–17979.

[40] G. Kresse, D. Joubert, From ultrasoft pseudopotentials to the projector augmented-wave method, *Phys. Rev. B* 59 (1999) 1758–1775.

[41] J.P. Perdew, K. Burke, M. Ernzerhof, Generalized gradient approximation made simple, *Phys. Rev. Lett.* 77 (1996) 3865–3868.

[42] J.K. Nørskov, T. Bligaard, A. Logadottir, J.R. Kitchin, J.G. Chen, S. Pandelov, U. Stimming, Trends in the exchange current for hydrogen evolution, *J. Electrochem. Soc.* 152 (2005) J23.

[43] Q. Wang, X. Zheng, Y. Deng, J. Zhao, Z. Chen, J. Huang, Stabilizing the α -phase of CsPb₃ perovskite by sulfobetaine zwitterions in one-step spin-coating films, *Joule* 1 (2017) 371–382.

[44] Z. Liang, Y. Xue, X. Wang, Y. Zhou, X. Zhang, H. Cui, G. Cheng, J. Tian, Co doped MoS₂ as cocatalyst considerably improved photocatalytic hydrogen evolution of g-C₃N₄ in an alkaline environment, *Chem. Eng. J.* 421 (2021), 130016.

[45] Y. Li, C. Gao, W. Jiang, C. Zhuang, W. Tan, W. Li, Y. Li, L. Wang, X. Liao, Z. Sun, J. Zou, X. Han, A game-changing design of low-cost, large-size porous cocatalysts decorated by ultra-small photocatalysts for highly efficient hydrogen evolution, *Appl. Catal. B: Environ.* 286 (2021), 119923.

[46] C. Gao, C. Zhuang, Y. Li, H. Qi, G. Chen, Z. Sun, J. Zou, X. Han, In situ liquid cell transmission electron microscopy guiding the design of large-sized cocatalysts coupled with ultra-small photocatalysts for highly efficient energy harvesting, *J. Mater. Chem. A* 9 (2021) 13056–13064.

[47] W. Tan, Y. Li, W. Jiang, C. Gao, C. Zhuang, CdS nanospheres decorated with NiS quantum dots as noble-metal-free photocatalysts for efficient hydrogen evolution, *ACS Appl. Energy Mater.* 3 (2020) 8048–8054.

[48] C. Zhuang, H. Qi, X. Cheng, G. Chen, C. Gao, L. Wang, S. Sun, J. Zou, X. Han, In-situ observation of dynamic galvanic replacement reactions in twinned metallic nanowires by liquid cell transmission electron microscopy, *Angew. Chem. Int. Ed.* 58 (2019) 18627–18633.